# Local Density Functional Study of Copper Clusters: A Comparison between Real Clusters, Model Surface Clusters, and the Actual Metal Surface

**Xavier Crispin,*[a] Christophe Bureau,*[b] Victor Geskin,[a] Roberto Lazzaroni,[a] and Jean-Luc Brédas*[a]**

**Keywords:** Copper clusters / Cu(100) surface / Chemical hardness / Relaxation energy / Size effect

Density Functional Theory is used to study the influence of the size of copper clusters modeling the Cu(100) surface, on the electronic properties: ionization potential, electron affinity, electronic chemical potential, and chemical hardness. The model clusters are chosen to have a bilayer structure and range in size from 9 to 20 copper atoms. The chemical hardness being identified as the relaxation energy of the frontier levels when an electron is removed or added to the system, a simple expression is proposed to estimate its value from the eigenenergies of the frontier levels in neutral and partially ionized systems. A detailed comparison of the geometric and electronic structures is made between the model surface copper clusters, real copper clusters, and the actual metal surface; it is seen that the model surface clusters provide an easy extrapolation to the properties of the metal surface.

## Introduction

Metal clusters are increasingly exploited as surface models to study surface reactions. The size dependence of their electronic properties and reactivities therefore attracts major interest from both fundamental and applied standpoints, especially since clusters provide a bridge between the properties of metal atoms and those of the infinite metallic solid, between homogeneous catalysis and heterogeneous catalysis.[1−6] To study the mesoscopic world between the metal atom and the metal solid, a traditional approach is to evaluate the properties of *real* metal clusters with intermediate sizes and to build a rationalization of the evolution of these properties. With real metal clusters, direct comparison between theory and experiment is possible; however, real clusters are shape-distorted spheres and thus present geometric structures (interatomic distances, packing structures) and electronic properties that can be much different from those of (infinite) metal surfaces. As we ultimately aim at studying reactions at metal surfaces, we have investigated size effects for metal clusters modeling metal surfaces; the geometric structure of such *model* clusters is chosen to represent a portion of the surface: they are flat (generally bilayered) and extended into two dimensions. The comparison between such an approach based on flat *model* clusters and the traditional approach using *real* clusters is interesting since both must extrapolate to the same limit at infinite size.

Among transition metal clusters, copper clusters are probably those that are most studied because of the apparent simplicity of the copper atom, which can be seen in a first approximation as monovalent (the 3d bonding and antibonding orbitals in a copper cluster are all filled). Numerous experimental measurements and theoretical studies of increasing sophistication have been performed on the size evolution of the properties of real copper clusters, such as ionization potential, electron affinity, and band gap.[7−12] Early theoretical approaches, such as the corrected classical model,[13] in which the cluster is considered as a perfect conducting sphere, fail to reproduce the behavior of electron affinity and ionization potential with cluster size.[14] Hence, a quantum mechanical treatment is needed to obtain a reliable average evolution of cluster properties, as shown in the semi-classical model of Brack.[14,15] The latter method is able to explore the properties of huge clusters (up to $10^6$ atoms) since the nuclei are not explicitly considered; however, it only gives an average evolution of the properties as a function of the cluster size, fails for small clusters, and does not provide other electronic features (bond description, charge distributions, etc.). The semi-classical model can be refined within jellium models to take into account shell effects, where the valence electrons move in a spherical or a perturbed spherical potential modeling the positive charge due to the nucleus screened by core electrons, such as the Clemenger−Nilsson model.[3,4,16] Such jellium methods reproduce the shell effect and even-odd oscillations typical of real copper clusters,[7,9,12] which are not explained by the classical or semi-classical models; however, they are not reliable for very small metallic clusters (< 7 atoms) since the nuclei cannot be modeled with a jellium. Methods that take into account the positions of the nuclei are therefore necessary; they are more computationally demanding but adequate to study small copper clusters. Among these are the effective-medium methods[17] and other semi-empirical methods[18,19] as well as Hartree−Fock ab initio methods[20−23] and density functional theory-based methods.[24−29]

In the first part of this work, a density functional approach is used to analyze the size evolution of electronic

[a] Service de Chimie des Matériaux Nouveaux, Centre de Recherche en Electronique et Photonique Moléculaires, Université de Mons-Hainaut,
Place du Parc 20, B-7000 Mons, Belgium
Fax: (internat.) + 32(0)65/37.33.66
E-mail: Xavier@averell.umh.ac.be
[b] DSM-DRECAM-SRSIM (bât 466), CEA-Saclay,
F-91191 Gif-sur-Yvette Cedex, France
Fax: (internat.) + 33-1/69.08.64.62
E-mail: bureau@DRECAM.cea.fr

  1434−1948/99/0202−0349 $ 17.50+.50/0 

properties (ionization potential and electron affinity) of copper clusters as surface models. In contrast to previous theoretical works,[23,24,28,29] the clusters studied here are designed to model an adsorption site of the Cu(100) surface. Therefore, copper cluster systems studied here do not have the quasi-spherical shape of real copper clusters. The consequences of such a difference are analyzed, on the one hand, on the validity of the surface model, and on the other hand, on the ability to extrapolate the evolution of ionization potential and electron affinity with cluster size.

In the second part, the copper clusters are characterized in terms of global properties as defined within Density Functional Theory (DFT): the electronic chemical potential ($\mu$) and chemical hardness ($\eta$). One of the highlights of the present work is to point out the relationship between hardness and relaxation energy of the valence levels when one electron is removed or added to the system; an estimate of hardness is proposed on the basis of the eigenenergies of the frontier levels of neutral and partially ionized systems. The evolutions of the chemical potential and hardness are analyzed with respect to the size of the clusters. Bureau et al.[30] have shown that the DFT chemical potential, $\mu$, is particularly relevant to describe the interaction of a molecule with a metallic surface, should it be polarized or not: $\mu$ is the pertinent parameter both for mimicking the setting of a metallic surface under voltage under electrochemical conditions, and for the description of the charge transfer between the adsorbed species and the surface. The latter aspect is based on the relationship between DFT and the Lewis concept of acids and bases, as introduced by Pearson and Parr;[31,32] within this scheme, the hardness of the surface and the molecule, and the difference in their chemical potentials are essential parameters for the understanding of adsorption phenomena.[32–34] It is thus of primary interest to analyze the behavior of these properties (chemical potential, chemical hardness) with cluster size since we ultimately aim at using metal clusters as surface models to study the interaction between an organic molecule and a metal surface.

We emphasize that we have deliberately chosen to adopt a very pedagogical pace to introduce the concepts touched upon in this work. The validity and merits of our methodological approach can in this way be best assessed.

## Methodology

### The (100) Copper Surface

An adsorption site of the fcc crystal (100) surface is modeled with various copper clusters by considering sizes ranging from nine to twenty copper atoms (Figure 1). The interatomic distances are fixed at the bulk crystal values, so that all reconstruction phenomena are neglected. This choice of interatomic distances for the copper clusters designed to model the surface is obviously taken to simulate at best a site on the surface. Indeed, it is well known that the atomic density at the surface and thus the interatomic distances can have a strong influence on the chemisorption energy of an adsorbate. This is illustrated by the different reactivities of different crystalline surfaces of transition metals.[35–37]

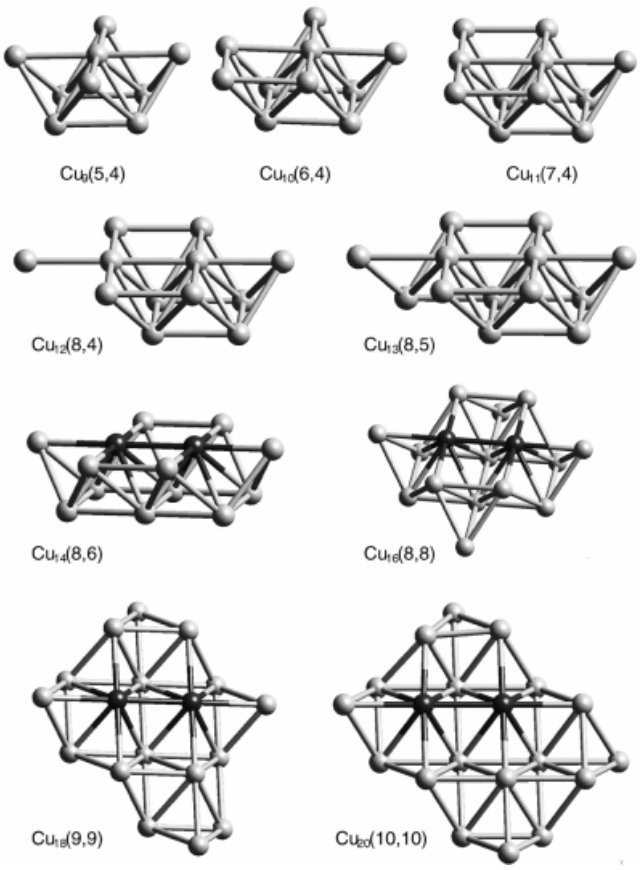


Figure 1. Representation of the copper clusters $Cu_n(y,w)$ used as models of the Cu(100) surface. The clusters are composed of two atomic layers; one containing $y$ atoms and the other $w$ atoms; from the fourteen-atom cluster, the two copper atoms in dark have the same nearest neighbors as a surface atom on the actual Cu(100) surface

The clusters are bilayered; the smallest one is $Cu_9(5,4)$ (where the subscript indicates the total number of copper atoms in the cluster and the numbers in parentheses denote the composition of its layers, in this case, 5 atoms in the upper layer and 4 in the bottom layer); in $Cu_9(5,4)$, the central atom of the upper layer has the same number of nearest neighbors as on the actual (100) surface. Clusters $Cu_{10}(6,4)$, $Cu_{11}(7,4)$, and $Cu_{12}(8,4)$ are obtained by extending the upper layer; extending the bottom layer then leads to $Cu_{13}(8,5)$ and $Cu_{14}(8,6)$; $Cu_{14}(8,6)$ has two central atoms which have the same number of nearest neighbors as on the actual (100) surface. Larger clusters built from $Cu_{14}(8,6)$ are also considered: $Cu_{16}(8,8)$, $Cu_{18}(9,9)$, and $Cu_{20}(10,10)$.

### Computational Approach

The calculations are performed in the framework of the density functional theory.[38,39] This method is a nonempirical approach, alternative to Hartree–Fock-based theories,

that presently enjoys a wide range of applications to chemical problems due to the possibility of including a significant part of the electron correlation energy; correlation is essential for a correct description of transition metal compounds. An extension of the Kohn−Sham theory describes the energy as a continuous function of the occupation of the monoelectronic levels;[40,41] this allows one to use fractional occupations to evaluate the derivatives of energy with respect to the number of electrons in the system. The evaluation of such derivatives is a way to estimate the electronic chemical potential and chemical hardness of copper clusters.

All the calculations were performed with the DMol program.[42,43] The basis set is DNP (double zeta numeric with polarization). The core orbitals are frozen during the SCF iterations and we choose a "MEDIUM" mesh size of the numerical grid for the calculations.[42,44,45] The calculations are performed within the local spin density approximation (LSD) with the Vosko−Wilk−Nusair exchange-correlation potential.[46] The ionization potential and electron affinity are calculated from total energy differences: $IP(n) = E_{tot}(Cu^+) - E_{tot}(Cu_n)$ and $EA(n) = E_{tot}(Cu_n) - E_{tot}(Cu^-_n)$ [note that, when using this convention, $EA(n) > 0$ means the anionic species is more stable than the neutral species]; the ions are maintained in the same geometry as the neutral copper clusters. The LSD approximation is known to give electron affinities and ionization potentials that are better than those obtained with Hartree−Fock methods[47,48] and in reasonable agreement with experimental data. Therefore, reliable trends for the evolution of electronic properties with respect to the size of the copper clusters can be expected from LSD calculations. Note that since the method is less computationally demanding than the gradient-corrected approximations, it allows us to consider relatively large clusters with all 3d, 4s and 4p atomic orbitals of Cu included in the basis set. The charge analysis used in this work comes from the Hirshfeld scheme, which is directly based on electronic density.[49,50]

## Results and Discussion

The presentation of the results is divided into two parts. Firstly, we compare the electronic properties of the model clusters [representing a site of the copper (100) surface] to those of real copper clusters; the evolution of ionization potential (*IP*) and electron affinity (*EA*) as a function of cluster size is analyzed. Secondly, the electronic chemical potential (μ) and the chemical hardness (η) of copper clusters are evaluated and their evolution with cluster size is discussed.

### Comparison between Real Copper Clusters, Surface-Model Clusters, and the Metal Surface

In this section, the $Cu_n(y,w)$ clusters modeling the Cu(100) surface are compared to the corresponding real clusters $Cu_n$, in terms of geometric structure and behavior of *EA* and *IP* with cluster size. The main geometric differences are the interatomic distances and the overall shape of the clusters; their consequences on the electronic properties are described below.

Small real copper clusters (<10 atoms) have significantly shorter interatomic distances[22,27,28] than those in the bulk (nearest-neighbor distance of 2.55 Å). The mean interatomic distance in real copper clusters tends to increase when the cluster grows. As far as the atomic packing is concerned, the fcc structure is found to be the most stable for clusters larger than thirteen atoms with interatomic distances close to those of the bulk metal.[51] Hence, the contraction of the interatomic distances is significant only for small clusters.

The interatomic distances used in the model clusters are the same as those in the bulk (thus larger than the distances of the corresponding real clusters), and their structure is fcc. Note that the use of non-optimized clusters has some unexpected consequences: in the spin-unrestricted calculations, some clusters with an even number of atoms are more stable in their triplet state, whereas real copper clusters with an even number of atoms are expected to be singlet. The total spin of the most stable states found in the odd-clusters (i.e., having an odd number of atoms), namely $Cu_9$(5,4), $Cu_{11}$(7,4), and $Cu_{13}$(8,5), is always 1/2. For the even-clusters, the spin of the most stable state is one for $Cu_{10}$(6,4), zero for $Cu_{12}$(8,4), one for $Cu_{14}$(8,6), one for $Cu_{16}$(8,8), and zero for $Cu_{18}$(9,9) and $Cu_{20}$(10,10). Nevertheless, it must be noted that the total energy of the first singlet state for $Cu_{10}$(6,4), $Cu_{14}$(8,6), and $Cu_{16}$(8,8) is always very close to that of the first triplet state. The fact that we obtain triplet states for these clusters results from the quasi-degeneracy of the one-electron levels near the highest occupied molecular orbital, which is a consequence of the large interatomic distances used and the non quasi-spherical symmetry of the clusters, as explained below.

The ionic species $Cu^-_n$ and $Cu^+_n$ used to calculate *EA*(*n*) and *IP*(*n*) are more stable in a state having a spin multiplicity of either one or two. The spin multiplicity is one for the anionic or cationic odd-clusters, and two when the ionic species have an even number of copper atoms. No spin-multiplicity difference among the charged even-clusters is observed, in contrast to the neutral clusters.

*1. Size Dependence of EA and IP:* We now consider the evolution of electron affinity and ionization potential with the size of copper clusters. These two properties are expected to converge on increasing the cluster size since both become equal to the workfunction at infinite size where the cluster is truly metallic, with no electronic gap. In Figure 2, we compare the *EA* values calculated for the $Cu_n(y,w)$ clusters to those measured experimentally from the ionization threshold of real anionic clusters.[7,9] In the experimental work, the energy needed to remove an electron from the anionic cluster was associated to the opposite of the electron affinity of the neutral cluster; as it is a vertical evaluation of *EA*, these experiments in fact provide the *EA* of the neutral cluster in the geometry of the anionic cluster. Note that the presence of an extra electron globally increases the interatomic distances; this is closer to our theo-

retical situation since the interatomic distances of the $Cu_n(y,w)$ clusters are those of the bulk (known to be larger than in small neutral clusters). It can be seen in Figure 2 that the theoretical values of *EA* and the experimental data lie in the same energy range; such an overall agreement is an indication of the ability of our method to evaluate *EA*.

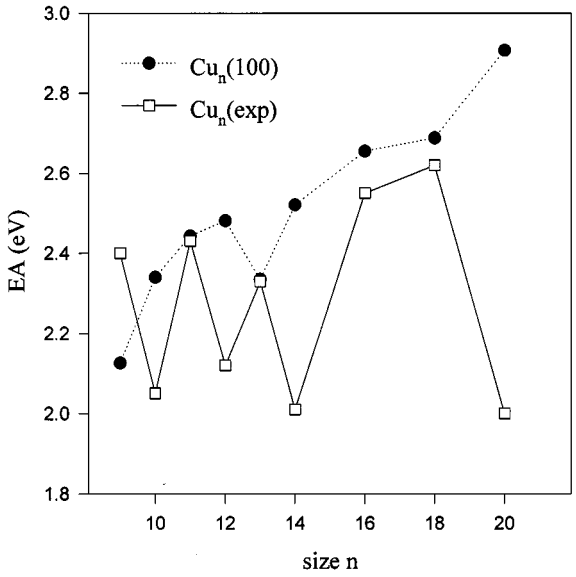


Figure 2. Comparison between the calculated electronic affinities (*EA*) of the copper clusters $Cu_n(y,w)$ ($n = 9 - 20$) modeling the (100) surface and the experimental values for the corresponding real copper clusters

Some errors are expected to be introduced by the LSD and frozen-core approximations used in our calculations. The magnitude of this error can be estimated by comparing the experimental vertical *EA* provided by ultraviolet photoelectron spectroscopy (UPS) measurements on the anionic copper dimer[8] to the calculated value $EA_{cal}$. $EA_{cal}$ is the difference between the total energy of the anionic copper dimer whose geometry was optimized and the total energy of the neutral copper dimer in the geometry of the anionic species. The experimental vertical *EA* of $Cu_2$ is 0.89 ±0.01 eV, while the calculated *EA* is 0.80 eV. That the error in the evaluation of the electron affinity for $Cu_2$ is small (0.1 eV), again illustrates the ability of the method we apply to calculate such a property.

The most striking feature of Figure 2 is the oscillating behavior of the experimental curve, which is not reproduced in the calculations. In order to understand this difference, it is necessary to briefly recall basic theoretical models describing real copper clusters. Real copper clusters (>7 atoms) tend to adopt an equilibrium geometry consisting of either a sphere or a distorted sphere. This was demonstrated theoretically for copper clusters up to 29 atoms by searching the most stable geometry using a simulated annealing approach coupled to an effective-medium method.[17] Although strong 3d-4s hybridization occurs for some small copper clusters, which affects their electronic structure and geometry,[27] it has been shown that the Cu−Cu bonds are mainly due to the overlap of 4s atomic orbitals, as mentioned for $Cu_2$.[26,52] Various theoretical studies aiming at explaining experimental data have used the following crude but reasonable approximation (e.g. refs.[9] and[12]): copper atoms are considered as monovalent in clusters; as a consequence, the number of valence electrons involved in a cluster is the same as the number of copper atoms in the cluster. In this approximation, the 4s valence electrons of an ideal spherical copper cluster are confined in a spherically symmetric potential (spherical jellium model). Because of its symmetry, such a potential gives rise to a spherical shell structure where the valence electrons successively fill the degenerate levels. The electronic system of a cluster with exactly the right number of electrons to complete a shell is very stable. This is the case when the number of 4s electrons is for instance 8 or 20; the corresponding clusters ($Cu_8$, $Cu_{20}$) are thus very stable: this is called the "shell effect" and the numbers 8 and 20 are called "magic numbers ($n_g$)". This can be experimentally related to the high relative abundance in the mass spectrum for the anionic species of ($n_g - 1$) atoms, like 7 and 19,[7,8] and for cationic species of ($n_g + 1$) copper clusters, like 9 and 21;[53] such stable ions have a completely filled shell. When one atom is added to a $Cu_8$ or $Cu_{20}$ neutral cluster, its valence electron occupies a degenerate state with considerably higher energy, and hence the stability of the cluster is reduced. In such a case, the cluster symmetry is reduced into a distorted sphere in order to minimize the energy (Jahn−Teller-like effect).[17,54] For each system, the structure distorts to maximize the gap at the Fermi level under the constraints set up by other energy contributions. For even-numbered clusters, there are two electrons in the HOMO and thus the energy gain due to the distortion is larger, resulting in a larger gap.[17] This interplay between the electronic system and the geometry of the cluster allows some clusters to be very stable without having a "magic number" of atoms.

As shown by Pettiette et al.,[9] the low electron affinity of magic-size copper clusters with respect to the *EA* of the neighboring sizes, as well as the even-odd oscillations of experimental *EA* values, can be explained qualitatively within a monoelectronic scheme with Koopmans' theorem thanks to jellium models:

(i) The sudden decrease in *EA* for magic sizes ($Cu_{20}$) can be understood by considering the shell structure appearing when valence electrons move in a spherical potential; the *EA* for $n = 20$ is lower than that for size $n - 1 = 19$, since an additional electron must occupy a new shell of higher energy. For surface models $Cu_n(y,w)$, no shell structure is expected since the shape is not spherical but flat. This explains why $Cu_{20}(10,10)$, corresponding to a magic size for real clusters, does not have a low calculated *EA*. As a consequence, *EA* for size 20 differs most importantly with respect to experiment (ca. 1 eV) (Figure 2).

(ii) The magnitude of the even-odd oscillations is about 0.5 eV in small real copper clusters; these oscillations decrease when the size increases and disappear at the bulk limit. To qualitatively understand the even-odd oscillations, Taylor et al.[12] refer to the case of monovalent, non-fully symmetrical clusters, thus with no degeneracy in the energy levels. In the even-numbered neutral clusters, the HOMO is

doubly occupied while the odd-numbered neutral clusters are open-shell species. To a first approximation, the extra electron, which makes the cluster negative, would either occupy the lowest unoccupied molecular orbital (LUMO) of the even-numbered clusters or fill the HOMO of the odd-numbered clusters. Such an effect will result into lower *EA* for the even-atom clusters.

The lack of even-odd oscillations in the theoretical curve (Figure 2) can be understood on the basis of the density of valence states (DOS) of the $Cu_n(y,w)$ surface models. The calculated DOS of the model $Cu_{10}(6,4)$ cluster and that of the real $Cu_{10}^{D_{4d}}$ cluster (both shown in Figure 3), as well as the experimental photoemission spectrum of Cu(100),[19,55] are presented in Figure 4 [the DOS of the copper clusters are obtained by enveloping the DFT eigenvalue spectrum with Gaussians of width 0.1 eV and we use Löwdin's decomposition[56] to obtain local DOS (LDOS); note also that the Fermi level is set at zero energy]. The comparison between these DOS and the experimental spectrum shows, on the one hand, strong differences between the DOS of $Cu_{10}^{D_{4d}}$ and that of $Cu_{10}(6,4)$, and, on the other hand, the similarity between the DOS of $Cu_{10}(6,4)$ and the experimental photoemission spectrum of Cu(100). For both copper clusters, the most important region of d monoelectronic states lies in the −4,0 to −1,3 eV range, between hybridized s-p states. Two main differences appear between the DOS of the two copper clusters: the global shape and the electronic gap. The DOS spectrum of the real cluster $Cu_{10}^{D_{4d}}$ shows weakly overlapping peaks, while the DOS of the 3 d states of $Cu_{10}(6,4)$ is non-vanishing in the entire −3 to −1 eV energy range, where these states are almost exclusively concentrated; these features are present in the total DOS of all $Cu_n(y,w)$ clusters studied here. The lower symmetry of $Cu_n(y,w)$ relative to spherical clusters, is responsible for the more uniform, in general, distribution of the monoelectronic states, i.e. the absence of the degenerate levels. The fact that the 3d states of $Cu_{10}(6,4)$ are mainly localized at higher energy is related to the chemical saturation (the number of the nearest neighbors) of the copper atoms in the clusters. Indeed, Figure 5 shows that the lower the saturation of the copper atoms, the more they are involved in 3d states of high energy: the local DOS corresponding to molecular orbitals involving 3d atomic orbitals centered on the peripheral atoms of the top layer (3 or 4 nearest neighbors) are mainly in a range of higher energy than the local DOS related to the peripheral atoms of the bottom layer (5 or 6 nearest neighbors); it is the local DOS related to the most saturated atom, i.e. the central atom with 8 nearest neighbors, that spreads over the widest range of energy. Hence, since every atom is saturated almost equally in $Cu_{10}^{D_{4d}}$, its DOS does not display the specific concentration of 3d valence states in a range of high energy as for $Cu_{10}(6,4)$.

The other main difference between the eigenvalue spectrum of $Cu_{10}^{D_{4d}}$ and that of $Cu_{10}(6,4)$ is the significant electronic gap for the real cluster (Figure 4), while for our surface model the electronic gap is vanishingly small; extremely small gaps are actually observed for all $Cu_n(y,w)$ surface models, since these clusters do not have spherical or quasi-spherical symmetry. This is why the evolution of $IP(n)$ and $EA(n)$ for these clusters does not show shell effects and even-odd oscillations. The removal of such strong oscillations in $EA(n)$ [and also in $IP(n)$] is actually a major advantage when the average behavior of these properties needs to be extrapolated to larger cluster sizes.

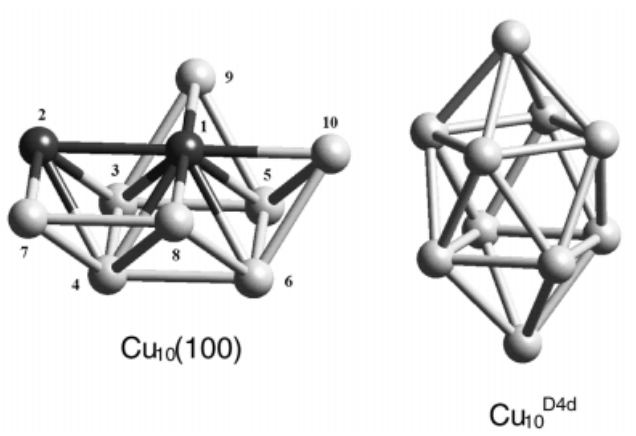


Figure 3. Geometric structures of the surface model $Cu_{10}(6,4)$ and of the corresponding real cluster $Cu_{10}^{D_{4d}}$

In Figure 4, we observe a narrower distribution of the 3d and 4s states in the DOS of $Cu_{10}(6,4)$, relative to that in the experimental spectrum of Cu(100). This is due to two major reasons: first, the model cluster is not large enough to represent the metal; secondly, the application of Koopmans' theorem is not strictly valid for the DFT eigenvalues, since Janak has shown that these eigenvalues rather correspond to the derivative of the total energy with respect to the occupation of orbitals[40]. However, the striking similarity between the DOS of $Cu_{10}(6,4)$ and the experimental spectrum for Cu(100), along with the difference relative to the DOS of $Cu_{10}^{D_{4d}}$, is a favorable argument for considering the $Cu_n(y,w)$ surface models appropriate (and better than real clusters) to model the (100) copper surface.

*2. Exploration of the Mesoscopic Size Copper Clusters:* Here, we take advantage of the weak oscillations observed in the evolution of $EA(n)$ and $IP(n)$ for the $Cu_n(y,w)$ surface models to explore the mesoscopic region. Properties of large copper clusters are thus deduced from the properties calculated for small model copper clusters.

It has been shown that the evolution of the properties of real clusters, such as the cohesive energy, ionization potential, and electron affinity, can be described with a convergent series whose variable is the number of atoms ($n$) in the cluster.[57] When neglecting high-order terms, the truncated expansion contains only one unknown coefficient (A) and shows that a property G($n$) evolves as a function of $n^{-1/3}$:

$$G(n) = G(\infty) + A \cdot n^{-1/3} \quad (1)$$

The exponent of $n$ is thought to be related to the ratio between the surface and the volume of the cluster, as suggested by Müller et al.[57]. The exponent is therefore ap-

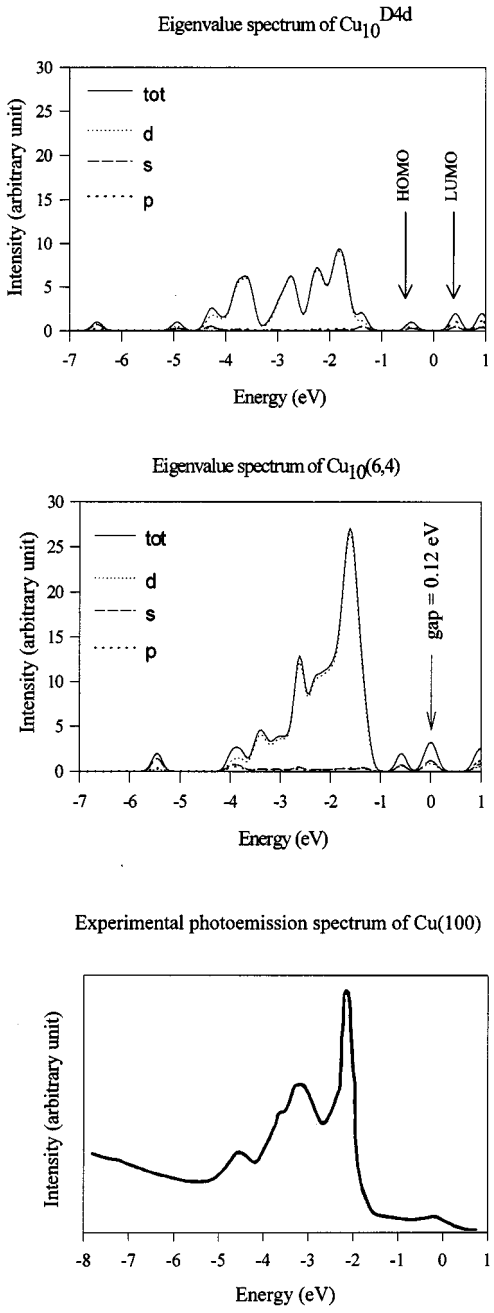


Figure 4. Comparison between the calculated total density of valence states (DOS) of $Cu_{10}^{D_{4d}}$, that of $Cu_{10}(6,4)$ and the experimental photoemission spectrum of Cu(100).[19,55] The total densities of valence states are enveloped with Gaussians of width 0.1 eV and their decomposition in local density of states (LDOS) is obtained from the scheme by Löwdin. The local density of states corresponding to molecular orbitals including 4s atomic orbitals is shown as a dashed line, the 4p component as a thick-dotted line and the 3d component as a thin-dotted line. The Fermi level is set at zero energy.

proximately −1/3 for real clusters, which are often almost spherical. Although the $Cu_n(y,w)$ surface models are not spherical, we also use −1/3 as the exponent, for the sake of simplicity and to allow a comparison with previous work dealing with real copper clusters[7−9,11]. The average behavior of $IP(n)$ or $EA(n)$ as a function of size ($n$) of the clusters can thus be expressed as follows: $EA(n) = W_{Cu} +$

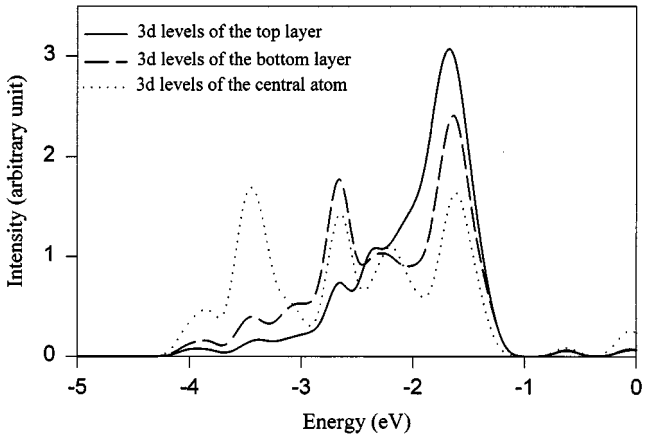


Figure 5. Local density of states (LDOS) from the d component of $Cu_{10}(6,4)$ localized on different regions of the cluster: (i) the peripheral atoms of the top layer (atoms labeled 2, 7, 8, 9, 10 in Figure 3) (full line); (ii) the peripheral atoms of the bottom layer (3, 4, 5, 6) (dashed line); and (iii) the central atom (1) (dotted line).

$B \cdot n^{-1/3}$ and $IP(n) = W_{Cu} + C \cdot n^{-1/3}$, where $W_{Cu}$ is the workfunction of polycrystalline copper (4.65 eV).

Accurate descriptions of the average evolution of $EA(n)$ and $IP(n)$ are obtained by imposing the condition that the curves $EA(n) = W_{Cu} + B{*}n^{-1/3}$ and $IP(n) = W_{Cu} + C \cdot n^{-1/3}$ pass through the experimental bulk limit ($n^{-1/3} = 0$, $W_{Cu} = 4.65$ eV), see Figure 6. Coefficients B and C are determined from linear regressions, which yields the following expressions:

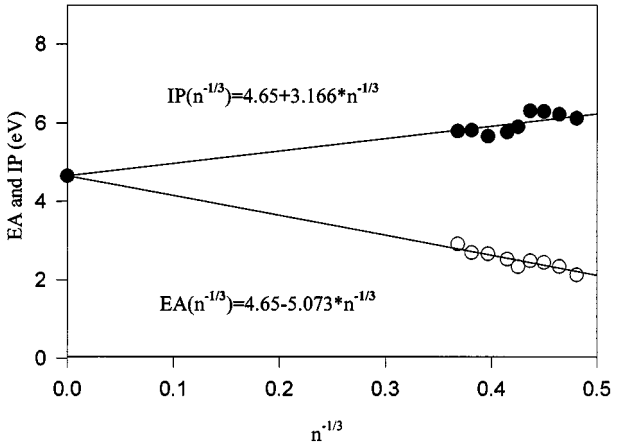


Figure 6. Evolution of calculated $EA(n)$ (open circles) and $IP(n)$ (full circles) with the size $n$ of the cluster $Cu_n(y,w)$. The straight lines represent the average evolution of these properties with size, as obtained by the method described in the text. The intersection point between the average evolution of $IP(n)$ and that of $EA(n)$ is set at the workfunction of polycrystalline copper ($W_{Cu} = 4.65$ eV).

$$EA(n) = 4.65 - 5.073 \cdot n^{-1/3} \quad (2a)$$

$$IP(n) = 4.65 + 3.166 \cdot n^{-1/3} \quad (2b)$$

Note that if the linear regressions are performed without imposing the curve to pass through ($n^{-1/3} = 0$, $W_{Cu} = 4.65$ eV), the extrapolated values for the workfunction of copper is found to be 4.34 eV; this is as good an estimate as those found for the workfunction of other metals from jellium calculations in the LSD approximation (VWN func-

tional).[58,59] Since oscillations are very weak for large copper clusters, the average evolution of $EA(n)$ or $IP(n)$ given by these expressions is expected to follow closely the real evolution. Therefore, we believe that calculations on small copper clusters can provide valuable estimates of the properties of large copper clusters, by means of the above interpolation formulae.

An argument in favor of the validity of the calculated coefficients is that the ratio between coefficient B for $EA(n)$ and C for $IP(n)$, i.e. B/C = −5.073/3.166, is very close to that observed in various experimental studies (−5/3)[8,11]. The average behavior of $IP(n)$ and $EA(n)$ can be evaluated from the limited sample of $Cu_n(y,w)$ ($n$ = 9−20) clusters studied here because the absence of spherical symmetry induces small electronic gaps and thus a rather linear evolution of $IP(n)$ and $EA(n)$ vs. $n^{-1/3}$. The simple expressions describing the average evolution of $IP(n)$ and $EA(n)$ will thus be used below to describe the behavior of the chemical potential of the clusters.

## Size Dependence of Chemical Potential μ(n) and Hardness η(n)

*1. Evaluation of Chemical Potential and Hardness; Relation with Other Electronic Properties:* The chemical potential and the hardness or softness of the clusters are important parameters for describing the physics and chemistry of metal clusters. Firstly, various studies have shown that the softness, a global property measuring the response of a system to the change in the number of electrons at fixed external potential, is directly related to the static dipole polarizability $\alpha$, a measure of the response of the electron cloud to the change in external potential (modification of external electric field) at a fixed number of electrons.[60−66] Secondly, the chemical potential and the hardness are related to the reactivity and the charge transfer between the metal cluster and an adsorbate upon chemical bond formation.[34,67] Moreover, Ghanty et al. noticed that the condition of maximum hardness, which can be regarded as a criterion of stability,[68] can in general be associated to the minimum polarizability.[69] Thus, the chemical reactivity could be guided by the evolution of hardness or polarizability upon reaction.

In this section, we show the relation between hardness and relaxation of valence levels when an electron is added or removed from the electronic system. We then propose various ways to estimate these properties and calculate the hardness $\eta(n)$ and chemical potential $\mu(n)$ for the $Cu_n(y,w)$ copper clusters.

We first consider a neutral cluster containing $n$ copper atoms, with $N_0$ electrons explicitly taken into account in the calculations; here, $N_0 = 11 \cdot n$, since 11 electrons per atom are not frozen. Janak showed that the DFT total energy can be seen as a continuous function of the occupation vector and thus of the number of electrons, $N$, in the system.[40] The total energy of $Cu_n^{+x}$, E($n$, $N = N_0 - x$), obtained by the removal of a negative charge $x|e|$ ($x$ is not necessarily an integer), can be expressed from the total energy of the neutral cluster, $E(n,N_0)$, by means of a series:[38,67]

$$E(n, N = N_0 - x) = E(n, N_0) - x\left(\frac{\partial E}{\partial N}\right)_{N=N_0} + (x^2/2)\left(\frac{\partial^2 E}{\partial N^2}\right)_{N=N_0} - R(x^3) \quad (3)$$

$R(x^3)$ contains the higher-order terms of the series. An analogous expression can be written when considering the addition of a partial charge $x$. We recall that, in DFT, the first derivative of the expansion, $(\delta E/\delta N)_{N = N_0}$, considering either charge removal or addition, is defined as the electronic chemical potential $\mu(n)$;[70] while half of the second derivative, $1/2(\delta^2 E/\delta N^2)_{N = N_0}$, corresponds to the absolute hardness[32] $\eta(n)$ or half of the inverse of the softness $[2S(n)]^{-1}$. The chemical potential, i.e., the opposite of the electronegativity, and the hardness can also be obtained in the finite difference approximation:[32]

$$\mu(n) \approx -\frac{IP(n) + EA(n)}{2} \; ; \quad \eta(n) \approx \frac{IP(n) - EA(n)}{2} \quad (4)$$

As discussed by several authors,[41,71−74] electronic open-shell systems have a single chemical potential while closed-shell systems do not have a unique chemical potential. Indeed, for the latter, the removed electron comes from the HOMO level while the added electron goes to the LUMO level. As a consequence, the derivative (at $x$ = 0) of the energy with respect to the charge removed from the system, i.e. the chemical potential denoted $\mu^+$, corresponds to the HOMO energy, according to Janak′s theorem;[40] similarly, the derivative of the energy with respect to the charge added to the system, i.e. $\mu^-$, corresponds to the LUMO energy.

$$\mu^+(n) = \left(\frac{\partial E(n,N)}{\partial(N_0 - x)}\right)_{N_0^+} = \varepsilon_{HOMO}(n, N_0) \quad (5a)$$

$$\mu^-(n) = \left(\frac{\partial E(n,N)}{\partial(N_0 + x)}\right)_{N_0^-} = \varepsilon_{LUMO}(n, N_0) \quad (5b)$$

For closed-shell systems, the injection of Equations 5 into Equation 3 allows the definition of the ionization potential and electron affinity:

$$IP(n) = E(n,N_0 - 1) - E(n,N_0) = -\varepsilon_{\mathrm{HOMO}}(n,N_0) + E^+_{\mathrm{rel}}(n) \quad (6a)$$
$$-EA(n) = E(n,N_0 + 1) - E(n,N_0) = \varepsilon_{\mathrm{LUMO}}(n,N_0) + E^-_{\mathrm{rel}}(n) \quad (6b)$$

$E^+_{\mathrm{rel}}(n)$ and $E^-_{\mathrm{rel}}(n)$ are the relaxation energy when an electron is removed from the HOMO level and the relaxation energy when an electron is added to the LUMO of the cluster of size $n$, respectively. The relaxation energies, as defined here, are expressed as follows:

$$E^+_{\mathrm{rel}(n)} = \eta^+(n) + R^+(n) = IP(n) + \varepsilon_{\mathrm{HOMO}}(n,N_0) \quad (7a)$$
$$E^-_{\mathrm{rel}(n)} = \eta^-(n) + R^-(n) = -EA(n) + \varepsilon_{\mathrm{LUMO}}(n,N_0) \quad (7b)$$

where $R^+(n)$ and $R^-(n)$ are the values of the higher-order terms $R(x^3)$ in the series (Eq. 3) for $x = 1$ when the electron is removed or added to the system, respectively:

$$R^+(n) = \sum_{i=3} \frac{(-1)^i}{i!} \left( \frac{\partial^i E}{\partial N^i} \right)_{N=N_0} \quad (8a)$$

$$R^-(n) = \sum_{i=3} \frac{1}{i!} \left( \frac{\partial^i E}{\partial N^i} \right)_{N=N_0} \quad (8b)$$

When $R^+(n)$ and $R^-(n)$ can be neglected, the relaxation energy of the valence levels is directly related to the hardness of the electronic system. In this approximation, *we propose a new expression for the hardness*, which can be written as:

$$\eta_{ED}{}^+(n) = \frac{1}{2} \left( \frac{\partial^2 E(n,N)}{\partial (N_0 - x)^2} \right)_{N_0^+} \cong IP(n) + \varepsilon_{HOMO}(n,N_0) \quad (9a)$$

$$\eta_{ED}{}^-(n) = \frac{1}{2} \left( \frac{\partial^2 E(n,N)}{\partial (N_0 + x)^2} \right)_{N_0^-} \cong -EA(n) - \varepsilon_{LUMO}(n,N_0) \quad (9b)$$

The hardnesses estimated using Equation 9 are denoted $\eta_{ED}(n)$, since the ionization potential and electron affinity are evaluated as total energy differences (ED).

The *IP* and *EA* values can also be calculated using Slater's transition state concept;[75–77] the simplest approach is to consider the opposite of the eigenenergy of the HOMO-[LUMO] coming from the neutral system, when this orbital is occupied by half of an electron, as the value of the ionization potential [electron affinity]. Consequently, the hardnesses of a system can be estimated only from the eigenvalues of the frontier orbitals for neutral and partially ionized systems:

$$\eta^-{}_{Slater}(n) \approx -\varepsilon_{HOMO}(n,N_0 - 1/2) - \varepsilon_{HOMO}(n,N_0) \quad (10a)$$
$$\eta^+{}_{Slater}(n) \approx -\varepsilon_{LUMO}(n,N_0 + 1/2) - \varepsilon_{LUMO}(n,N_0) \quad (10b)$$

Since, for the copper clusters we study here, the HOMO −LUMO gap is very small (as discussed above), we may consider in a first good approximation that unique (average) first and second derivatives of the energy can satisfactorily characterize the chemical potential and absolute hardness of the copper clusters (closed-shell and open-shell). Hence, the HOMO and LUMO eigenenergies written in the above relations can be replaced by the chemical potential of the copper clusters. This approximation becomes increasingly accurate for closed-shell systems as the size of the cluster expands, the electronic structure then approaching that of the metal, for which the chemical potential of the electrons and hardness are well-defined concepts[33]. Taking this approximation and neglecting the high-order terms $R(x^3)$ of the series in Eq. 3, the total energy difference, $[E(n, N_0 - x) - E(n, N_0)]$, displays a parabolic dependence on charge $x$:

$$[E(n,N_0 - x) - E(n.N_0)] = -\mu(n)x + \eta(n)x^2 \quad (11)$$

For $x = -1|e|$ and $x = 1|e|$, i.e. in the finite-difference approximation, Equation 11 provides $EA(n)$ and $IP(n)$ values that can be recombined to express $\mu(n)$ and $\eta(n)$ as in Equation 4. In order to improve on the accuracy of $\mu(n)$ and $\eta(n)$ with respect to the definitions given in Equation 4, we have considered a set of charges $x$ ($x = -1|e|$; $x = -0.5|e|$; $x = 0|e|$; $x = 0.5|e|$; $x = 1|e|$) and interpolated the SCF total energy difference $[E(n,N_0 - x) - E(n,N_0)]$ through the second-order polynomial of Equation 11, for each size $n$ of the clusters. The chemical potential and hardness of $Cu_n(y,w)$ clusters resulting from the above interpolation are denoted below $\mu(n)$ and $\eta(n)$ (without any indices).

Figure 7 shows the calculated $[E(n,N_0 - x) - E(n,N_0)]$ for $Cu_{20}(10,10)$ carrying different charges, together with the second-order fit. The value of the first derivative of this expression for $x = 0$ gives an estimate of the electronic chemical potential of the cluster $[-\mu(20)]$ while the curvature of the parabola (Eq. 10) is an estimate of the hardness of the cluster $[\eta(20)]$. The graph of Figure 7 provides the values of *EA*, *IP*, and $\mu$ for $Cu_{20}(10,10)$: respectively 2.9 eV, 5.8 eV, and −4.4 eV. We obtain the trend that the differences between $IP(20)$ and $-\mu(20)$ or between $-EA(20)$ and $\mu(20)$ are mainly related to the hardness $\eta(20)$ and only weakly depend on the higher terms $R$ in the expressions 7a and 7b: $\{IP(20) - [-\mu(20)]\} = 1.43$ eV and $[-\mu(20) - EA(20)] = 1.45$ eV are both very close to the curvature of the parabola $\eta(20) = 1.44$ eV.

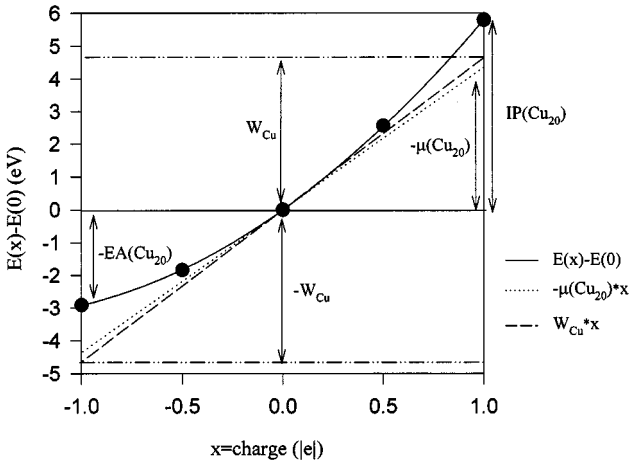


Figure 7. Calculated total energy of $Cu_{20}(10,10)$ as a function of charge $x$ (full circles). The parabola interpolated from the calculated points (Equation 11) is represented by a full line. The dotted line represents the tangent of the parabola at the origin, which corresponds to $[-\mu(Cu_{20}) \cdot x]$, and the dashed line represents $[W_{Cu} \cdot x]$. The arrows point to specific values, such as $IP(Cu_{20})$, $EA(Cu_{20})$, and $\mu(Cu_{20})$.

We now apply the relations defined above and compare the results to those obtained from the interpolation using Equation 11. Table 1 lists the energies of the HOMO and LUMO levels as a function of cluster size as well as the chemical potentials estimated from the slope at the origin of the interpolated parabola (Eq. 11). The $\mu$ values are very close to the HOMO or LUMO energies of the neutral $Cu_n(y,w)$ clusters. This confirms that Equation 11 is a

reasonable way to determine the chemical potential [we note that both frontier orbital energies are given in Table 1 since: (i) the calculations were performed at the unrestricted level; and (ii) the copper clusters having an even number of atoms are not necessarily closed-shell systems].

Table 1. Comparison between the chemical potential $\mu(n)$, estimated as the slope at the origin of the interpolated parabola described by Equation 11, and the eigenenergies of the frontier orbitals of the neutral copper clusters $Cu_n(y,w)$ with $n = 9-20$. All the electronic properties are given in eV.

| $n$ | $\mu(n)$ | $\varepsilon_{HOMO}(n,N_0)$ | $\varepsilon_{LUMO}(n,N_0)$ |
|---|---|---|---|
| 9 | −4.13 | −4.13 | −4.02 |
| 10 | −4.29 | −4.30 | −4.18 |
| 11 | −4.37 | −4.41 | −4.26 |
| 12 | −4.36 | −4.51 | −4.19 |
| 13 | −4.12 | −4.16 | −4.03 |
| 14 | −4.16 | −4.18 | −4.15 |
| 16 | −4.17 | −4.21 | −4.07 |
| 18 | −4.25 | −4.23 | −4.17 |
| 20 | −4.36 | −4.41 | −4.38 |

Table 2 compares the energies of the frontier levels when they are occupied by half an electron with the electron affinity and ionization potential coming from total energy differences. The results show that the use of Slater's transition state gives the right order of magnitude for the ionization potential and electron affinity. However, this simple approximation introduces some inaccuracy in the estimates of *EA* [err$|EA - \varepsilon_{LUMO}| = 0.28$ eV] and *IP* [err$|IP - \varepsilon_{HOMO}| = 0.14$ eV] and, consequently, also in Equations 10 which gives the hardness $\eta_{Slater}$.

Table 2. Comparison between the electron affinity (*EA*) and ionization potential (*IP*) of the $Cu_n(y,w)$ clusters, calculated using total energy differences and with the eigenenergies of the HOMO and LUMO levels occupied by half of an electron and coming from those of the neutral system (Err is the mean error). All the electronic properties are given in eV.

| $n$ | $EA(n)$ | $\varepsilon_{LUMO}(n,N_0 + 1/2)$ | $IP(n)$ | $\varepsilon_{HOMO}(n,N_0 - 1/2)$ |
|---|---|---|---|---|
| 9 | 2.13 | −2.82 | 6.12 | −6.22 |
| 10 | 2.34 | −2.38 | 6.22 | −6.13 |
| 11 | 2.44 | −3.06 | 6.29 | −5.97 |
| 12 | 2.48 | −2.42 | 6.31 | −6.20 |
| 13 | 2.33 | −2.77 | 5.90 | −5.75 |
| 14 | 2.52 | −2.54 | 5.77 | −5.81 |
| 16 | 2.66 | −2.46 | 5.66 | −5.67 |
| 18 | 2.69 | −2.60 | 5.82 | −5.83 |
| 20 | 2.91 | −3.26 | 5.79 | −6.21 |
| Err $\|EA - \varepsilon_{LUMO}\| = 0.28$ eV $\|IP - \varepsilon_{HOMO}\| = 0.14$ eV | | | | |

In Table 3, we compare the hardness values calculated in various ways. These all provide the right order of magnitude. However, the results from Equation 10 miss what appears as the reasonable evolution of the relaxation energy and hardness, i.e. their decrease with cluster size; it is likely that an improved approximation, such as the Generalized Slater's Transition State method,[76] would give the right evolution.

A relationship between the polarizability and the electronic relaxation of valence levels also exists since, as we have mentioned above, the hardness is related to the polarizability. In fact, a low relaxation energy implies a low energy cost of the deformation of the electronic cloud. Hence, the smaller the relaxation energy of valence molecular orbitals, the smaller the hardness and the higher the polarizability of the system.

Table 3. Comparison among: (i) the hardness, $\eta$, evaluated as the curvature of the interpolated parabola described by Equation 11; (ii) the hardness, $\eta^+_{ED}$ and $\eta^-_{ED}$, estimated from Equations 9a and 9b; and (iii) the hardness, $\eta^+_{Slater}$ and $\eta^-_{Slater}(n)$, coming from Equations 10a and 10b. The values are in eV.

| $n$ | $\eta^+_{ED}(n)$ | $\eta^-_{ED}(n)$ | $\eta^+_{Slater}(n)$ | $\eta^-_{Slater}(n)$ | $\eta(n)$ |
|---|---|---|---|---|---|
| 9 | 1.99 | 1.89 | 2.09 | 1.20 | 2.00 |
| 10 | 1.92 | 1.84 | 1.83 | 1.80 | 1.96 |
| 11 | 1.89 | 1.82 | 1.57 | 1.20 | 1.93 |
| 12 | 1.80 | 1.71 | 1.69 | 1.77 | 1.91 |
| 13 | 1.74 | 1.69 | 1.59 | 1.26 | 1.79 |
| 14 | 1.59 | 1.63 | 1.63 | 1.61 | 1.62 |
| 16 | 1.45 | 1.41 | 1.46 | 1.61 | 1.48 |
| 18 | 1.58 | 1.48 | 1.60 | 1.57 | 1.57 |
| 20 | 1.39 | 1.47 | 1.81 | 1.12 | 1.44 |

*2. Evolution of the Chemical Potential and Hardness with the Size of Copper Clusters:* The knowledge of the chemical potential and hardness of the copper clusters allows us to characterize the evolution of these properties with size, from a small metal cluster to bulk metal. Since the relationship between hardness, polarizability, and relaxation energy of the valence levels has been pointed out above, we also discuss the evolution of these properties.

The evolution of the parameters $\mu$ and $\eta$ of the parabola (Equation 11) has been analyzed as a funtion of the size of the cluster. The results are presented in Figure 8. We first discuss the behavior of the first derivative in the expansion, $-\mu(n)$. Figure 8 indicates that $-\mu$ remains close to the value of $W_{Cu}$ whatever the size; it slowly converges towards the workfunction of the metal surface for an infinite size, as found within the jellium model.[78] The oscillation of the chemical potential of the metal clusters is weaker than that of *IP* or *EA* since the chemical potential can be seen as an average of these properties (Eq. 4). Hence, the slope of the average evolution of $IP(n)$, $EA(n)$ and $-\mu(n)$ should also be correlated. The average evolutions were found above for $EA(n) = 4.65 - 5.073 \cdot n^{-1/3}$ and $IP(n) = 4.65 + 3.166 \cdot n^{-1/3}$. The slope $D$ of $-\mu(n) = 4.65 - D \cdot n^{-1/3}$ can be directly evaluated by using the interpolation formulae (Eq. 2) of $IP(n)$ and $EA(n)$ in Equation 4; it appears that $D = (5.073 - 3.166)/2 = 0.954$, which is in good agreement with the value of $D = 0.938$ calculated from a linear regression of $-\mu(n)$ for $n = 9-20$:

$$-\mu(n) = 4.65 - 0.954 \cdot n^{-1/2} \quad (12)$$

The small value of coefficient $D$ leads to a relatively weak dependence of $\mu$ on $n$, in the range of $n$ studied; this rationalizes the proximity between $-\mu$ and $W_{Cu}$ and the slow convergence of $-\mu$ towards $W_{Cu}$, i.e. the quasi-constant character of $\mu$ in the clusters studied here. The HOMO energy of copper clusters (Table 1), and thus the chemical potential as calculated here (since the gap is very small), is then a

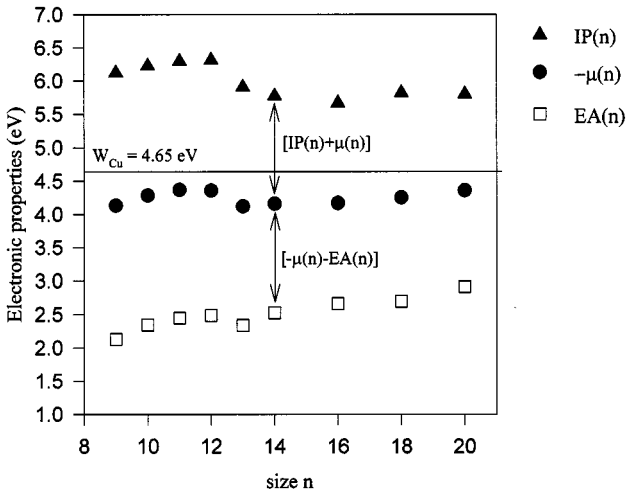


Figure 8. Evolution of the electronic properties of $Cu_n(y,w)$ with size *n*: (i) opposite of the chemical potential $-\mu(n)$ (full circles); (ii) $IP(n)$ (full triangles); and (iii) $EA(n)$ (open squares). The solid line indicates the workfunction of the metal.

good approximation of the workfunction of the metal. This result was first observed by Russier et al. for other transition metal clusters such as those of palladium.[79]

The hardness, $\eta(n)$, decreases as a function of size of the cluster (Figure 9). This trend is similar to that found for sodium clusters ($Na_n$).[63,65] The curvature of the parabola $\eta(n)$ (represented in Figure 7 for $n = 20$) decreases with increasing size *n*, hence the edges of the parabola for $x = -1$ and 1, i.e. *EA* and *IP* respectively, tend to become equal to the workfunction *W*, as shown in Figure 6. The decrease in hardness with cluster size is fully consistent with the expected evolution of the polarizability and relaxation energy. As the copper clusters grow, the number of valence levels that are close in energy increases, which induces a smaller relaxation energy and a higher polarizability.[63,80]

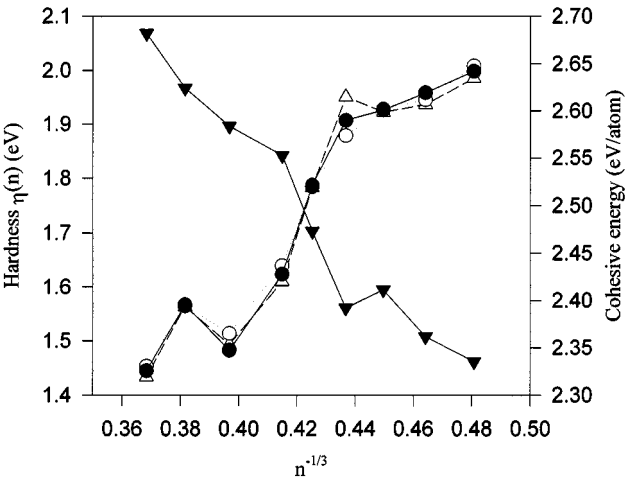


Figure 9. Evolution of the cohesive energy per atom (full triangles) and chemical hardness of the copper clusters $Cu_n(y,w)$. The full circles represent the hardness evaluated from the curvature of the polynomial expression (Eq. 11, Figure 7); the other two curves represent the evolution of $[IP(n) + \mu(n)]$ (open triangles) and $[-\mu(n) - EA(n)]$ (open circles).

For bulk metals, *n* is considered to be infinite and the relaxation energy when removing an electron at the Fermi energy is zero [for $n = \infty$, *IP* becomes the workfunction and the HOMO level corresponds to the Fermi level; Equation 7a then becomes: $E^+_{rel}(n = \infty) = 0$]. Equation 7a shows that the non-zero value of the hardness of a metal surface exactly corresponds to the opposite of the higher-order terms in the series of Eq. 3, $-R^+(n = \infty)$. Hence, as the hardness is also the inverse of the density of states at the Fermi level $g(E_F)$,[33] we obtain the following equalities:

$$\eta(n = \infty) = -R^+(n = \infty) = 1/[2g(E_F)] \quad (13)$$

This shows the direct relationship, for a bulk metal, between the higher-order terms in the series of Eq. 3 and the density of states at the Fermi level.

It has been demonstrated that hardness modifications with size are related to the shell structure in atoms or metal clusters.[65,81] The hardness of real copper clusters possessing a magic size is expected to be larger than that of the neighboring sizes, as observed for $Li_n$ clusters;[82] clusters with a magic size adopt a geometric structure such that a shell is filled, so that hardness is maximized according to the maximum hardness principle.[68] Consequently, as for the other properties [$IP(n)$, $EA(n)$], the absence of shell structure in the model copper clusters can be advantageous to evaluate the average evolution of hardness with size. Figure 9 indicates that the $[-\mu(n) - EA(n)]$ and $[IP(n) + \mu(n)]$ curves are similar to that of $\eta(n)$; this shows that the simple relation (Eq. 4) defining the hardness from *EA* and *IP* is valuable for finite copper clusters $Cu_n(y,w)$. Of course, Equation 4 is not valid for infinite metal clusters (according to it, the hardness would be zero, whereas the hardness of a metal is non-zero); nevertheless, since the hardness of a metal is small [$g(E_F)$ is large], it is reasonable to use Equations 4 and 2 to estimate the hardness of large clusters; injecting Equation 1 into 3 gives the following relation:

$$\eta(n) = 4.120 \cdot n^{-1/3} \quad (14)$$

The comparison between the evolutions of chemical potential (Eq. 12) and hardness (Eq. 14) illustrates that the hardness varies much more strongly than the chemical potential with size. In the expression of the total energy as a series (Eq. 3), it is the second-derivative term, related to the relaxation energy (Eq. 8) and hardness, that is mostly responsible for the variation of $IP(n)$ and $EA(n)$ when the size *n* is changed, as already indicated for *IP* by Russier[41].

We have also calculated the cohesive energy of the $Cu_n(y,w)$ copper clusters (binding energy per atom); it is found to evolve in a roughly linear manner with respect to $n^{-1/3}$ (Figure 9). This is in good agreement with the previous study by Delley et al. on quasi-spherical copper clusters.[25] Figure 9 clearly shows that when the cluster size increases, the cohesive energy increases while the hardness decreases. The same kind of observation was made by Ghanty et al.[63] for $Na_n$ clusters; these authors pointed out a polarizability increase as well as a cohesive energy increase with size of the $Na_n$ clusters. To the best of our

knowledge, no analytical relation between cohesive energy and hardness has been established. Such a relationship would probably be linked to another concept (which is not related to size dependence): the maximum hardness principle,[68] which is a stability criterion and could be associated to a minimum polarizability condition, as has been suggested by Ghanty.[69]

## Synopsis

Density Functional Theory has been used to study the dependence of the size of copper clusters $Cu_n(y,w)$ ($n$ = 9−20) modeling the Cu(100) surface on their electronic properties. A comparison has been made between real quasi-spherical clusters, flat clusters modeling the surface, and the actual metal surface. We can draw the following major conclusions:

(i) The electronic structure of the copper clusters modeling the surface involves the absence of shell effect and even-odd oscillation in the evolution of *EA* and *IP* with size. Consequently, the evolution of *IP* and *EA* with $n^{-1/3}$ is quasi-linear, which allows the extrapolation of these properties to large copper clusters, for which such DFT calculations are intractable.

(ii) The DOS analysis of the model $Cu_{10}(6,4)$ cluster, compared to that of the quasi-spherical $Cu_{10}^{D_{4d}}$, shows that the absence of shell structure in the flat copper clusters is due to their geometric structure. The DOS of the surface-modeling clusters are similar to the photoemission spectrum of the actual Cu(100) surface, indicating the better adequacy of such surface models to simulate the metal surface, compared to real copper clusters.

(iii) Another important feature of the electronic structure of the $Cu_n(y,w)$ model surfaces is the small HOMO-LUMO gap. This allows one to consider energy derivatives with respect to charge removal or addition to be equal for closed-shell systems. Hence, it is possible to define global properties such as the chemical potential, μ, and the absolute hardness, η, whatever the size and the closed or open shell character. These properties are estimated as derivatives of the total energy versus charge, where the energy function is a second-order polynomial interpolated from SCF total energies calculated for partially negatively and positively charged clusters.

(iv) By exploiting the newly established relationship between hardness and relaxation energy of the valence levels when an electron is added to or removed from the system, it becomes possible to estimate the hardness from the eigenenergies of the frontier levels of the neutral and partially ionized systems.

(v) The average evolutions of the chemical potential and hardness can be extrapolated vs. $n^{-1/3}$ from the expressions of *IP* and *EA* vs. $n^{-1/3}$. The chemical potential of small copper clusters is close to the workfunction of a polycrystalline copper surface and is already a good estimate of this macroscopic property. The hardness decreases significantly with size; this is directly related to the decrease in relaxation energy of the valence levels and the increase in polarizability when increasing the size towards the metal.

In a forthcoming paper, we intend to exploit the knowledge base obtained in the present work to study the influence of the copper cluster size on the adsorption of organic molecules such as acrylonitrile; the adsorption of acrylonitrile on copper surfaces and copper electrodes has indeed been identified as the initial step leading to the grafting of polyacrylonitrile on a copper cathode through electropolymerization, a process that holds much promise for the surface protection of commodity metals.[83−85]

## Acknowledgments

The Mons−Saclay collaboration is conducted in the framework of the "TOURNESOL" bilateral programme between Belgium and France (contract 98.026). The work in Mons is partly supported by the Belgian Federal Government "Service des Affaires Scientifiques, Techniques et Culturelles (SSTC)" in the framework of the "Pôle d'Attraction Interuniversitaire en Chimie Supramoléculaire et Catalyse Supramoléculaire (PAI 4/11)", FNRS-FRFC, and an IBM Academic Joint Study. XC is a grant holder of "Fonds pour la Formation à la Recherche dans l'Industrie et dans l'Agriculture (FRIA)". RL is Maître de Recherches of the Belgian "Fonds National de la Recherche Scientifique (FNRS)".

[1] G. Schmid, *Chem. Rev.* **1992**, *92*, 1709−1727.
[2] R. S. Berry, *Chem. Rev.* **1993**, *93*, 2379−2394.
[3] W. A. d. Heer, *Rev. Mod. Phys.* **1993**, *65*, 611−676.
[4] M. Brack, *Rev. Mod. Phys.* **1993**, *65*, 677−732.
[5] H. Haberland (Ed.) *Clusters of Atoms and Molecules*, Springer Series in Chemical Physics, 52 (Germany, **1995**).
[6] J. Shi, S. Gider, K. Babcock, D. D. Awschalom, *Science* **1996**, *271*, 937−941.
[7] L. S. Zheng, C. M. Kraner, P. J. Brucat, S. H. Yang, C. L. Pettiette, M. J. Craycraft, R. E. Smalley, *J. Chem. Phys.* **1986**, *85*, 1681−1688.
[8] D. G. Leopold, J. Ho, W. C. Lineberger, *J. Chem. Phys.* **1987**, *86*, 1715−1726.
[9] C. L. Pettiette, S. H. Yang, M. J. Craycraft, J. Conceicao, R. T. Laaksonen, O. Cheshnovsky, R. E. Smalley, *J. Chem. Phys.* **1988**, *88*, 5377−5382.
[10] M. F. Jarrold, K. M. Creegan, *Int. J. Mass Spectrom. Ion Processes* **1990**, *102*, 161−181.
[11] J. Ho, K. M. Ervin, W. C. Lineberger, *J. Chem. Phys.* **1990**, *93*, 6987−7002.
[12] K. J. Taylor, C. L. Pettiette, O. Cheshnovsky, R. E. Smalley, *J. Chem. Phys.* **1992**, *96*, 3319−3329.
[13] G. Makov, A. Nitzan, L. E. Brus, *J. Chem. Phys.* **1988**, *88*, 5076−5085.
[14] M. Seidl, K. H. Meiwes-Broer, M. Brack, *J. Chem. Phys.* **1991**, *95*, 1295−1303.
[15] M. Brack, *Phys. Rev. B* **1989**, *39*, 3533−3542.
[16] K. Clemenger, *Phys. Rev. B* **1985**, *32*, 1359−1362.
[17] O. B. Christensen, K. W. Jacobsen, J. K. Norskov, M. Manninen, *Phys. Rev. Lett.* **1991**, *66*, 2219−2222.
[18] R. C. Baetzold, R. E. Mack, *J. Chem. Phys.* **1975**, *62*, 1513−1520.
[19] A. B. Anderson, *J. Chem. Phys.* **1978**, *68*, 1744−1751.
[20] C. Bachmann, J. Demuynck, A. Veillard, *Faraday Symp.* **1980**, *14*, 170−179.
[21] J. Demuynck, M. M. Rohmer, A. Strich, A. Veillard, *J. Chem. Phys.* **1981**, *75*, 3443−3453.
[22] J. Flad, G. Igelmann, H. Preuss, H. Stoll, *Surf. Sci.* **1985**, *156*, 379−385.
[23] D.-W. Liao, K. Balasubramanian, *J. Chem. Phys.* **1992**, *97*, 2548−2552.
[24] R. P. Messmer, S. K. Knudson, K. H. Johnson, J. B. Diamond, C. Y. Yang, *Phys. Rev. B* **1976**, *13*, 1396−1415.

[25] B. Delley, D. E. Ellis, A. J. Freeman, E. J. Baerends, D. Post, *Phys. Rev. B* **1983**, *27*, 2132−2144.
[26] G. S. Painter, F. W. Averill, *Phys. Rev. B* **1983**, *28*, 5536−5547.
[27] K. Jackson, *Phys. Rev. B* **1993**, *47*, 9715−9722.
[28] C. Massobrio, A. Pasquarello, R. Car, *Chem. Phys. Lett.* **1995**, *238*, 215−221.
[29] P. Calaminci, A. M. Köster, N. Russo, D. R. Salahub, *J. Chem. Phys.* **1996**, *105*, 9546−9556.
[30] C. Bureau, G. Lécayon, *J. Chem. Phys.* **1997**, *106*, 8821−8829.
[31] R. G. Pearson, *J. Am. Chem. Soc.* **1963**, *85*, 3533−3539.
[32] R. G. Parr, R. G. Pearson, *J. Am. Chem. Soc.* **1983**, *105*, 7512−7516.
[33] W. Yang, R. G. Parr, *Proc. Natl. Acad. Sci. USA*. **1985**, *82*, 6723−6726.
[34] R. F. Nalewajski, *J. Am. Chem. Soc.* **1984**, *106*, 944−945.
[35] C. F. Zinola, A. J. Arvia, G. L. Estiu, E. A. Castro, *J. Phys. Chem.* **1994**, *98*, 7566−7576.
[36] S. Seong, A. B. Anderson, *J. Phys. Chem.* **1996**, *100*, 11744−11747.
[37] J. T. Stuckless, C. E. Wartnaby, N. Al-Sarraf, S. J. B. Dixon-Warren, M. Kovar, D. A. King, *J. Chem. Phys.* **1997**, *106*, 2012−2030.
[38] R. G. Parr, W. Yang, *Density-Functional Theory of Atoms and Molecules*; Oxford University Press (New York, **1989**).
[39] D. P. Chong, *Recent Advances in Density Functional Methods*; World Scientific (Singapore, **1995**), Vol. 1.
[40] J. F. Janak, *Phys. Rev. B* **1978**, *18*, 7165−7168.
[41] V. Russier, *Phys. Rev. B* **1992**, *45*, 8894−8901.
[42] B. Delley, *J. Chem. Phys.* **1990**, *92*, 508−517.
[43] B. Delley, *New. J. Chem.* **1992**, *16*, 1103−1107.
[44] D. Ellis, G. Painter, *Phys. Rev. B.* **1968**, *56*, 2887−2895.
[45] Biosym/MSI. DMol 95.0/3.0.0, *Quantum Chemistry User Guide* (San Diego, **1995**).
[46] H. Vosko, L. Wilk, M. Nusair, *Can. J. Phys.* **1980**, *58*, 1200−1211.
[47] T. Ziegler, *Chem. Rev.* **1991**, *91*, 651−667.
[48] R. O. Jones, O. Gurnnarsson, *Rev. Mod. Phys.* **1989**, *61*, 689−746.
[49] F. L. Hirshfeld, *Theoret. Chim. Acta.* **1977**, *44*, 129−138.
[50] B. Delley, *Chem. Phys.* **1986**, *110*, 329−338.
[51] P. A. Montano, G. K. Shenoy, E. E. Alp, W. Schulze, J. Urban, *Phys. Rev. Lett.* **1986**, *56*, 2076−2079.
[52] E. A. Rohlfing, J. J. Valentini, *J. Chem. Phys.* **1986**, *84*, 6560−6566.
[53] I. Katakuse, T. Ichihara, Y. Fujita, T. Matsuo, T. Sakurai, H. Matsuda, *Int. J. Mass Spectrom. Ion Processes* **1985**, *67*, 229−236.
[54] M. Brack, O. Genzken, K. Hansen, *Z. Phys.* **1990**, *D 19*, 51−53.
[55] J. M. Burkstrand, G. G. Kleiman, G. G. Tibetts, J. C. Tracy, *J. Vac. Sci. Tech.* **1976**, *13*, 291−295.
[56] P. O. Löwdin, *J. Chem. Phys.* **1950**, *18*, 365−375.
[57] H. Müller, H. G. Fritsche, L. Skala, Chap 2.5: Analytic Cluster Models and Interpolation Formulae for Clusters Properties, In *Clusters of Atoms and Molecules I*; Haberland, H., (Germany, **1995**); pp 114−140.
[58] Z. Y. Zhang, D. C. Langreth, J. P. Perdew, *Phys. Rev. B* **1990**, *41*, 5674−5684.
[59] R. Monnier, J. P. Perdew, *Phys. Rev. B* **1978**, *17*, 2595−2611.
[60] P. J. Politzer, *J. Chem. Phys.* **1987**, *86*, 1072−1073.
[61] A. Vela, J. L. Gazquez, *J. Am. Chem. Soc.* **1990**, *112*, 1490−1492.
[62] J. K. Nagle, *J. Am. Chem. Soc.* **1990**, *112*, 4741−4747.
[63] T. K. Ghanty, S. K. Ghosh, *J. Phys. Chem.* **1993**, *97*, 4951−4953.
[64] T. K. Ghanty, S. K. Ghosh, *J. Phys. Chem.* **1994**, *98*, 9197−9201.
[65] S. Hati, D. Datta, *J. Phys. Chem.* **1994**, *98*, 10451−10454.
[66] S. Hati, D. Datta, *J. Phys. Chem.* **1995**, *99*, 10742−10746.
[67] W. J. Mortier, S. K. Ghosh, S. Shankar, *J. Am. Chem. Soc.* **1986**, *108*, 4315−4320.
[68] R. G. Parr, P. K. Chattaraj, *J. Am. Chem. Soc.* **1991**, *113*, 1854−1857.
[69] T. K. Ghanty, S. K. Ghosh, *J. Phys. Chem.* **1996**, *100*, 12295−12298.
[70] R. G. Parr, R. A. Donnelly, M. Levy, W. E. Palke, *J. Chem. Phys* **1978**, *68*, 3801−3807.
[71] J. P. Perdew, R. G. Parr, M. Levy, J. L. Balduz, *Phys. Rev. Lett.* **1982**, *49*, 1691−1694.
[72] R. G. Parr, L. J. Bartolotti, *J. Phys. Chem.* **1983**, *87*, 2810−2815.
[73] J. Cioslowski, B. B. Stefanov, *J. Chem. Phys.* **1993**, *99*, 5151−5162.
[74] M. H. Cohen, M. V. Ganduglia-Pirovano, J. Kudrnovsky, *J. Chem. Phys.* **1994**, *101*, 8988−8997.
[75] J. C. Slater, *Adv. Quantum Chem.* **1972**, *6*, 1.
[76] A. R. Williams, R. A. deGroot, C. B. Sommers, *J. Chem. Phys.* **1975**, *63*, 628−631.
[77] D. P. Chong, *Chem. Phys. Lett.* **1995**, *232*, 486−490.
[78] E. Engel, J. P. Perdew, *Phys. Rev. B* **1991**, *43*, 1331−1337.
[79] V. Russier, D. R. Salahub, C. Mijoule, *Phys. Rev. B.* **1990**, *42*, 5046−5056.
[80] D. E. Beck, *Phys. Rev. B* **1984**, *30*, 6935−6942.
[81] R. Parr, Z. Zhou, *Acc. Chem. Res.* **1993**, 256−258.
[82] M. K. Harbola, *Proc. Natl. Acad. Sci. USA* **1992**, *89*, 1036−1039.
[83] G. Lécayon, Y. Bouizem, C. Le Gressus, C. Reynaud, C. Boiziau, C. Juret, *Chem. Phys. Lett.* **1982**, *91*, 506−510.
[84] C. Bureau, G. Deniau, P. Viel, G. Lécayon, J. Delhalle, *J. Adhesion* **1996**, *58*, 101−121.
[85] X. Crispin, R. Lazzaroni, V. Geskin, N. Baute, P. Dubois, R. Jérôme, J. L. Brédas, *J. Am. Chem. Soc.*, in press.

Received August 27, 1998
[I98292]